Research article

Assessment of particulate matter and inorganic gaseous pollutants in Bou-Ismail, Tipaza City, Algeria, including levels and health risks

Adlane Tahar[1,2], Abdelkader Lemou[1,2], Lyes Rabhi[1,2*], Nabila Cherifi[1,2], Riad Ladji[1,2]

[1]Centre de Recherche Scientifique et Technique en Analyses Physico-chimiques (CRAPC), Bou-Ismail, Tipaza, Algeria
[2]Unité de Recherche en Analyses Physico-Chimiques des Milieux Fluides et Sols (URAPC-MFS/ CRAPC), Ben Aknoun – Alger, Algeria
*Corresponding author: rabhilyes@live.fr

Received: 9 May 2025 - **Reviewed:** 4 July 2025 - **Accepted:** 4 November 2025
https://doi.org/10.17159/caj/2025/35/2.21575

Abstract

This research presents a comprehensive evaluation of air pollution levels linked to vehicular traffic in Bou-Ismail using a statistical methods to examine correlations, trends, and relationships between pollutant concentrations and meteorological variables, as well as to assess factors contributing to particulate pollution in the Bou-Ismail area. A monitoring station was established along a major roadway for six months from December 16, 2015, to June 29, 2016, to assess particulate matter ($PM_{2.5}$ and PM_{10}), ozone, sulphur dioxide, carbon monoxide, nitrogen oxides, and volatile organic compounds to investigate the factors and variables that contribute to particulate pollution in the Bou-Ismail area. The average concentrations of SO_2 and NO_2 for the campaign were equal to 0.14 and 12.07 ppb, respectively, respecting the national guidelines. Concentration in this study for PM_{10} and $PM_{2.5}$ were 20.2 and 8.9 µg/m^3. The predictive models applied to evaluate particulate matter concentrations demonstrated strong performance, yielding coefficient of determination (R^2) values exceeding 0.83. No correlation was seen between PM and WS (wind speed), while O_3 concentration was positively correlated with temperature. PC1 (35.38%) indicates that cars contribute the most to local air pollution, with significant particle and petrol emissions but low VOCs. PC2 (21.75%) relates CO to vehicles, while buildings have the most VOCs, followed by transport and agriculture. The $PM_{2.5}$ Air Quality Index (AQI) exceeded guideline thresholds on more than 42 days out of 196 days recorded, which indicates that the air quality is unhealthy to very unhealthy for sensitive groups. The hazard quotient (HQ) in our investigation was below 1, which signifies a tolerable level of risk. The average monthly ELCR (Excess lifetime cancer risk) of $PM_{2.5}$ in this research surpassed the recommended guideline value of 1.0E-06. According to HYSPLIT back-trajectory investigations, western European air pollution reached western Algeria via Portugal and southern Spain. Mauritanian air masses may have carried Saharan dust to Mali and south Algeria. The second to last phase saw eastern Algiers air masses migrate north into the Mediterranean, signifying pollution export. $PM_{2.5}$ and PM_{10} concentrations increase in westerly and southerly airflows.

Keywords

Health outcomes; road traffic; air quality index; excess lifetime cancer risk

Introduction

In recent years, urban air pollution has grown because of the expansion of transportation sectors, rapid urbanisation, industrialisation, and motorisation (Rani Hemamalini et al. 2022; Wu et al. 2023). This induces serious health risks, particularly in older adults and the disabled. Due to the potential for increased concentrations and epidemiological data suggesting that exposure to air pollutants in the near-roadway environment increases the risk of cardiorespiratory mortality and morbidity, air pollution is a concern (Valavanidis et al. 2006; Santus et al. 2012). As reported by the World Health Organization, there were about 4.2 million deaths worldwide in 2016 attributable to ambient air pollution caused by conditions including stroke, heart disease, lung cancer, lower respiratory infections, and chronic obstructive pulmonary disease (WHO 2022). To help their citizens, several nations have instituted systems for tracking and reporting air quality, and concentrations of various air pollutants in various regions of the globe, such as PM, CO, NO_x, SO_2, have been measured by several tracking programs.

Photochemical smog relies largely on ozone (O_3) in the troposphere. It harms humans via contact with the skin, eyes, and lungs (Iglesias-Suarez et al. 2020; Li et al. 2021). It is produced by photochemical reactions involving NO_x and VOC emissions, both natural and anthropogenic, and the action of UV radiation, making it a secondary pollutant. The link between O_3 and its precursors (NO_x and VOCs) displays extremely non-linear interactions due to the complicated chemical process and geographical variances in emission distribution and meteorology (Li et al. 2021).

Oxides of nitrogen (nitric oxide (NO) and nitrogen dioxide (NO_2) are both in the definition of NO_x. Most nitrogen oxides (NO_x) originate from automobiles, factories, power plants, and other large-scale fuel-burning facilities. Storms, forest fires, and human-caused food production are only a few of the natural causes. When released into the atmosphere, NO may oxidise to generate NO_2, but releases much more NO (Wu et al. 2023). Carbon monoxide (CO) is a perfect indicator of the accumulation extent since it is chemically stable in ambient air at ground level (Shen et al. 2022) and produced by the combustion of fossil fuels, fires in forests, and garbage management. CO harms humans by efficiently competing with oxygen in the blood of binding sites with the haem part of blood cells, decreasing the blood's capacity to transport oxygen to vital organs like the heart and brain (Thurston 2008).

As PM emissions from various sources are characterised by particles in varying size ranges, determining the relative dominance of fine mode (or coarse mode) particulates across an area is of paramount relevance in explaining these sources. Fine particulates are emitted or formed from a variety of sources, including burning fossil fuels, vehicle emissions, industrial operations, gas-to-particle conversion (most of these relate to human activities), and so on. Coarse particles are made up mostly of PM emitted through operations, including mining, quarrying, and agriculture, as well as fugitive emissions, wind erosion, desert dust, and other sources generally correlated to natural activities (Spandana et al. 2021).

$PM_{2.5}$ and PM_{10} are Group I carcinogens, according to the International Agency for Research on Cancer, and they harm public health. Increased $PM_{2.5}$, PM_{10}, SO_2, NO_2, and ground-level O_3 concentrations originate from sources like industrial operations and combustion processes (Mushtaq et al. 2024). The respiratory system is vulnerable to the harmful effects of air pollution. Sulfur dioxide, nitrogen oxides, and ozone in high concentrations have been linked to many health problems, including nasal and throat irritation, coughing, chest pain from airway constriction, and increased mucus production on the walls of the upper airways, which can trigger inflammatory reactions and, in extreme cases, asthma and chronic obstructive pulmonary disease (Guarnieri and Balmes 2014).

The Air Quality Index (AQI) is a useful tool for the general public to quickly gauge the air quality around them and make informed decisions about pollution control strategies and indoor air quality management (Verma et al. 2016). The U.S. Environmental Protection Agency (USEPA, 1999) uses the same technique to calculate the AQI, which is defined as an index or rating scale for measuring the daily cumulative impact of ambient air pollutants seen in the tracking locations. Many epidemiological studies show that acute or chronic PM exposure increases mortality and morbidity. The World Health Organization (WHO) has recommended annual standard limits of 15 µg/m^3 for PM_{10} and 5 µg/m^3 for $PM_{2.5}$, with corresponding 24-hour limits of 45 µg/m^3 and 15 µg/m^3, respectively, to prevent harmful health impacts (WHO 2021).

Many researchers use risk assessments to evaluate the elevated risk among individuals exposed to varying concentrations of hazardous air pollution. A health risk assessment helps characterise the likely negative effects of pollutant exposure. This prediction program uses measured exposure data to estimate pollutant health impacts. This research used USEPA's risk assessment approach to estimate health risks from inhalation for all ages. People who breathe in $PM_{2.5}$ were given an Extraordinary Lifetime Cancer Risk (ELCR) and a non-carcinogenic risk to their health methods (Sidibe et al. 2022; Saju et al. 2023). Its observed significant temporal variations in PM_{10}, $PM_{2.5}$, and NO_x/SO_2 concentrations at the Bou-Ismail urban site, noting distinct seasonal peaks during winter heating periods and increased photochemical activity in summer (Lemou et al. 2020).

Through this contribution, we present the results obtained during continuous sampling in Algeria's urban (coastal) area from December 2015 to June 2016. This work is being done because it is hard to limit regional air quality models. There is not enough good information on PM and gases in Algeria and the southern Mediterranean area. Understanding the amounts and risks of particulate matter, which can be found using methods for evaluating human health risks, can help government officials, environmental and health experts, and others take effective steps to protect and improve people's health in this megacity. This study will help decision-makers to enforce or enhance current policies that reduce the release of harmful pollutants into the atmosphere or implement risk management techniques. Based on the large bibliographic research we have carried out, we judge that the information in this database will be a regional standard to measure the effects of rising human-made emissions, contributions from sources, and the importance of atmospheric processes.

Material and methods

Monitoring site and period

The observation experiment was conducted from December 16, 2015, to June 29, 2016. The sample location coordinates in Bou-Ismail are 36° 64'15" N, 2° 71'81" E. The sample location is 45 km east-west of Algiers, in the eastern section of the Tipaza area, and 3 km east of Bou-Ismail (population: 70,000) (Supplementary material, Figure S1, showing the map of Bou-Ismail sampling

stations used in the study). This area is a highly populated urban area. The regional leader in paper processing, Tonic, is headquartered in this city's vibrant industrial zone, within fifty metres of the sample location and heavy car traffic. Receptors should be positioned 5 or 25 metres closer to the road source, according to the US EPA (USEPA 2023). However, this study was based on a single ambient air monitoring station positioned along a major roadway in Bou-Ismail. Since only one sampling location was used, there was no spatial separation between the multiple samplers.

Data on an hourly basis for air pollutants was absent due to electricity outages and other technical difficulties at the sampling location. Of the total 4729 hours over the study months, 3923 hourly measures were recorded, yielding the following completion rates for each month: December (99%), January (54%), February (98%), March (93%), April (100%), May (100%), and June (97%). The hourly readings were transformed into daily averages and considered absent if over one-third of the day's data was missing from the commencement of collection on December 15 to March 31, 2016 (Winter), and from April 1, 2016, to June 29, 2016 (Spring).

System monitoring

The measurements were conducted using a single compact multi-gas air quality monitoring system (Airpointer® by Recordum) deployed at the roadside sampling location in Bou-Ismail. The Airpointer® is the instrument for continuously monitoring volatile and gaseous ambient concentrations from combustion processes along a perimeter. Its sensors for the standard reference technique can detect CO, O_3, SO_2, and NO/NO_2/NO_x across a wide range of concentration levels. As an open platform, it allows for simply integrating more sensors. The Airpointer® offers continuous real-time data, allowing for swift and wise action in the event of an accident (Details on the instrumentation, calibration procedures, and measurement techniques are provided in Supplementary material, Text 1). The limits of detection (LOD) for the Airpointer are as follows, according to manufacturer standards and site verification: $PM_{2.5}$: about 1–2 µg/m^3, NO_2: approximately 2–3 ppb, O_3: approximately 2 ppb, CO: approximately 0.1 ppm, VOC (if applicable): approximately 5–10 ppb (contingent on chemical and sensor).

Raw values of $PM_{2.5}$ and PM_{10} were adjusted using a multivariate linear regression model derived from co-location data, which incorporated temperature and relative humidity factors. The correction model produced an R^2 of 0.86 for $PM_{2.5}$ (RMSE = 3.9 µg/m^3) and an R^2 of 0.79 for PM_{10} (RMSE = 5.6 µg/m^3). The modification was consistently applied to the time series for the site. More details are provided in the Supplementary material, Text 1.

Air mass trajectories

The Hybrid Single-Particle Lagrangian Integrated Trajectory Model (HYSPLIT), developed by the National Oceanic and Atmospheric Administration/The Air Resources Laboratory (NOAA/ARL), was used to pilot the air mass trajectories that arrived at the sampling location. This model was fed by the Global Data Assimilation System (GDAS), which has a spatial resolution of 1° × 1°. The approach has been used to determine the origin and path of particulate matter at the site of measurement (Rabhi et al. 2024). The frequency charts are calculated by dividing the trajectories by the total intersections in each grid cell. The HYSPLIT model was used, which integrates Lagrangian and kinetic information from a single particle. At an altitude of 500m, a 120-hour backwards trajectory study was conducted (Rolph et al. 2017). The 120-hour HYSPLIT backwards trajectories were selected to ensure a wide range of long-distance transport routes, particularly for particulate matter (PM) and inert tracers that can stay in the atmosphere for several days. This period might be more extended than how long some short-lived species (like VOCs or NO_2) last in the atmosphere; however, the longer time frame was used to include regional effects and the history of how pollutants attached to PM or secondary pollutants are moved around.

Statistical analysis

Pearson Correlation Analysis (PA), Hierarchical Cluster Analysis (HCA), and Principal Component Analysis (PCA) are used first to identify several sources of Bou-Ismail (The statistical methods applied, including PCA, Pearson correlation, and hierarchical cluster analysis, are described in Supplementary material, Text 2).

Air quality index

The AQI, developed in the United States and adopted by other nations throughout the globe, is the most popular (Gladson et al. 2022). The AQI is a significant metric used to assess the extent of air pollution. The AQI measurements are categorised into six classifications: good, moderate, unhealthy for sensitive groups, unhealthy (for the general population), very unhealthy (triggering health alerts for the entire population), and hazardous (emergency conditions affecting everyone) (USEPA 2009). The primary pollutants used to evaluate air quality are $PM_{2.5}$, PM_{10}, SO_2, NO_2, O_3, and CO. The sub-index is determined by selecting the highest value as the AQI value, which quantitatively represents the AQI of the respective location. Their estimate is directly related to the concentration of a certain pollutant in the air.

The AQI is a useful tool for communicating air quality to the public (Chen et al. 2018). The concentrations of five categories of criterion pollutants—O_3, PM, CO, SO_2, and NO_2—are aggregated into a singular metric referred to as the AQI. This composite indicator condenses intricate data from several pollutants into a singular value, facilitating understanding of overall air quality conditions for the public and policymakers. It evaluates the potential health hazards of air pollution by indicating the pollutant with the highest risk level on a specific day. To better understand the contribution of each pollutant to the overall air quality, we calculated individual AQI values for five categories of pollutants. The index scale is divided into broad areas corresponding to health education messaging

(AQI classifications and their associated health risk levels are summarized in Supplementary material, Text 3). However, the US EPA uses an identical method to get the AQI. Parameter-specific formulae are used to determine the AQI as:

$$Ip = [I_{Hi} - I_{Lo} / BP_{Hi} - BP_{Lo}] * (Cp - BP_{Lo}) + I_{L} \quad (1)$$

Where: Ip = index of pollutant p. Cp = truncated concentration of pollutant p. BP_{Hi} = concentration breakpoint, i.e. greater than or equal to Cp. BP_{Lo} = concentration breakpoint, i.e., less than or equal to Cp. I_{Hi} = AQI value corresponding to BP_{Hi}. I_{Lo} = AQI value corresponding to BP_{Lo}.

For the tracking site under consideration, the dominant AQI value will be the one with the highest value among the current sub-indices used for calculation; this value is taken from the report (2).

$$AQI = \max(I_{O3}, I_{PM2.5}, I_{PM10}, I_{CO}, I_{SO2}, I_{NO2}) \quad (2)$$

Air pollution and the resulting health risks go up with increasing AQI values (Supplementary material, Table S1, which describes the six-level classification system of AQI used in the study). AQI levels of 100 or less are considered good. Air quality is considered harmful when AQI values exceed 100, first for certain vulnerable groups of individuals and then for everyone as AQI values continue to rise. Six categories make up the AQI (AQI classifications and their associated health risk levels are summarized in Supplementary material, Text 3). Varying health concerns relate to each category. Each group also has a unique colour. Thanks to the colour, people can immediately identify whether the air quality in their neighbourhoods has reached harmful levels.

Several nations and regions use an AQI (Lanzafame et al. 2015; Sarkar et al. 2022; Zhang and Li 2022; Cusick et al. 2023; Khoshakhlagh et al. 2023; Bamola et al. 2024), typically starting at the urban scale, to convey information about air quality. These include the United Kingdom (UK), the United States of America (USA), Belgium, France, Spain, Finland, Sweden, Canada, Mexico, Australia, New Zealand, Hong Kong, Singapore, Malaysia, Thailand, China, Macau, Indonesia, and Taiwan. The ambient concentrations of SO_2, PM_{10}, NO_2, CO, and O_3 are the primary basis for the AQI. $PM_{2.5}$ is included in the index's computation in a subset of circumstances. Most systems evaluate population exposure to air pollutants based on actual measurements (tracking data) rather than estimates (derived from models).

Health risk assessment

Health risk assessment is important for characterising the potential harmful effects of human exposure to a specific pollutant (Yunesian et al. 2019). This method is inherently predictive and utilises measured exposure data to determine the health impacts of human exposure to contaminants (Mehdi Qasemi and Allahdadi 2019). The United States Environmental Protection Agency (USEPA) established the risk assessment approach in this research, which focused on calculating health risks through inhalation for all age demographics (Yunesian et al. 2019). To evaluate the danger to human health from inhalation exposure to $PM_{2.5}$ and PM_{10} in Bou-Ismail ambient air, excess lifetime cancer risk (ELCR) and non-carcinogenic risk were calculated. The age-specific health risk assessment categorises the population into ten age groups (from birth to less than one year and 71 years and older) (Supplementary material, Table S2, listing risk assessment parameters for different age groups, including inhalation rates, exposure times, and RfDs). ELCR levels were considered safe for humans within the range of 1×10^{-5} to 1×10^{-6}. However, the USEPA recommends values below 1×10^{-6} (Heydari et al. 2019; Saju et al. 2023; Amare et al. 2024). The ELCR of PM_{10} was not calculated without the inhalation unit risk of PM_{10}. We computed the ELCR using the following equation:

$$ELCR = LADD\ (\text{lifetime average daily dose}\ (\mu g/kg.day)) \times SF\ (\text{slope factor}\ (kg.day/\mu g)) \quad (3)$$

The calculation of ELCR is directly affected by the excess lifetime average daily dose (LADD) and the slope factor (SF).

Reference analogous research from various regions that have employed international values in response to data deficiencies (Heydari et al. 2019; Saju et al. 2023; Amare et al. 2024). The ELCR was not calculated for PM_{10} because a specific slope factor (SF) for this pollutant was not available (USEPA 2011). This signifies a constraint of the current investigation, as PM_{10} is a significant pollutant with established health effects, including possible carcinogenicity. Future research should focus on gathering sufficient data on PM_{10} exposure to facilitate thorough risk evaluations. ELCRs were assessed at Bou-Ismail monitoring sites across 10 age groups, based on ground-based data. The United States Environmental Protection Agency (USEPA) defines an acceptable excess lifetime cancer risk (ELCR) for the general populace as typically ranging from 1 in 1,000,000 (1.0×10^{-6}) to 1 in 100,000 (1.0×10^{-5}), with risks exceeding 1 in 10,000 (1.0×10^{-4}) deemed significant enough to necessitate prompt regulatory intervention (USEPA 2011). The lifetime average daily dose (LADD) is used for substances having carcinogenic or chronic effects. The LADD represents the lifetime-averaged dose rate. The contaminant concentration denotes the level of contamination present in breathed air. Exposure duration denotes the cumulative time a person encounters an air contaminant. The LADD can be calculated using equation (4):

$$LADD = (C * IR * ED * EF) \div (AT * BW) \quad (4)$$

In this context, C denotes pollutant concentration ($\mu g/m^3$), IR represents inhalation rate (m^3/day), ED signifies exposure length (years), EF indicates exposure frequency (days/year), BW refers to body weight (kg), and AT stands for average exposure time (days).

The USEPA's Integrated Risk Information System (IRIS) presents the slope factor (SF) for each pollutant.

$$SF = BW \div (UR * IR) \quad (5)$$

SF is the slope factor, and UR is a unit risk (µg/m^3).

Obtaining the unit risk for $PM_{2.5}$ is necessary to calculate the SF value. No information is available on $PM_{2.5}$ in Algeria. This study used the risk unit value of $PM_{2.5}$ (0.008 µg/m^3) as stated by Greene and Morris (Greene and Morris 2006). However, prior investigations did not supply the unit risk and slope factor for PM_{10}, so we could not calculate the ELCR and carcinogenic risk for PM_{10}.

The hazard quotient (HQ) is utilised to evaluate the non-carcinogenic risk posed by a specific pollutant to the population of an area, calculated as the ratio of the average daily dose (ADD) to the reference dose (RfD), as described in Equation 6 (Supplementary material, Table S2, listing risk assessment parameters for different age groups including inhalation rates, exposure times, and RfDs) (U.S. EPA 2009 ; Mushtaq et al. 2024).

$$HQ \text{ (hazard quotient)} = LADD \text{ (lifetime average daily dose)} \div RfD \text{ (reference dose (µg/kg.day))} \quad (6)$$

If HQ surpasses 1, the potential risk may be considerable. HQ ≤ 1 signifies a tolerable level of risk (Yunesian et al. 2019; Saju et al. 2023; Amare et al. 2024). Absent data about the RfC for $PM_{2.5}$ and PM_{10}, we used an RfC value of 15 µg/m^3 for diesel particles to calculate the reference dose (RfD) for $PM_{2.5}$ and an RfC of 50 µg/m^3 for PM_{10} (Supplementary material, Table S2, listing risk assessment parameters for different age groups, including inhalation rates, exposure times, and RfDs) to assess the potential for adverse health effects (Saju et al. 2023).

Results and discussion

Overview of pollutant concentrations and meteorological variables

The weather station was used to collect the weather data in Figure 1. During the sampling period, temperatures fluctuated between 7.7 °C and 26.5°C, averaging 16.4 °C. Wind speed ranged from 0.3 to 4.1 m/s, with an average of 1.7 m/s. The direction of the wind (>53%) was mainly from the southwest quadrant (180–270°).

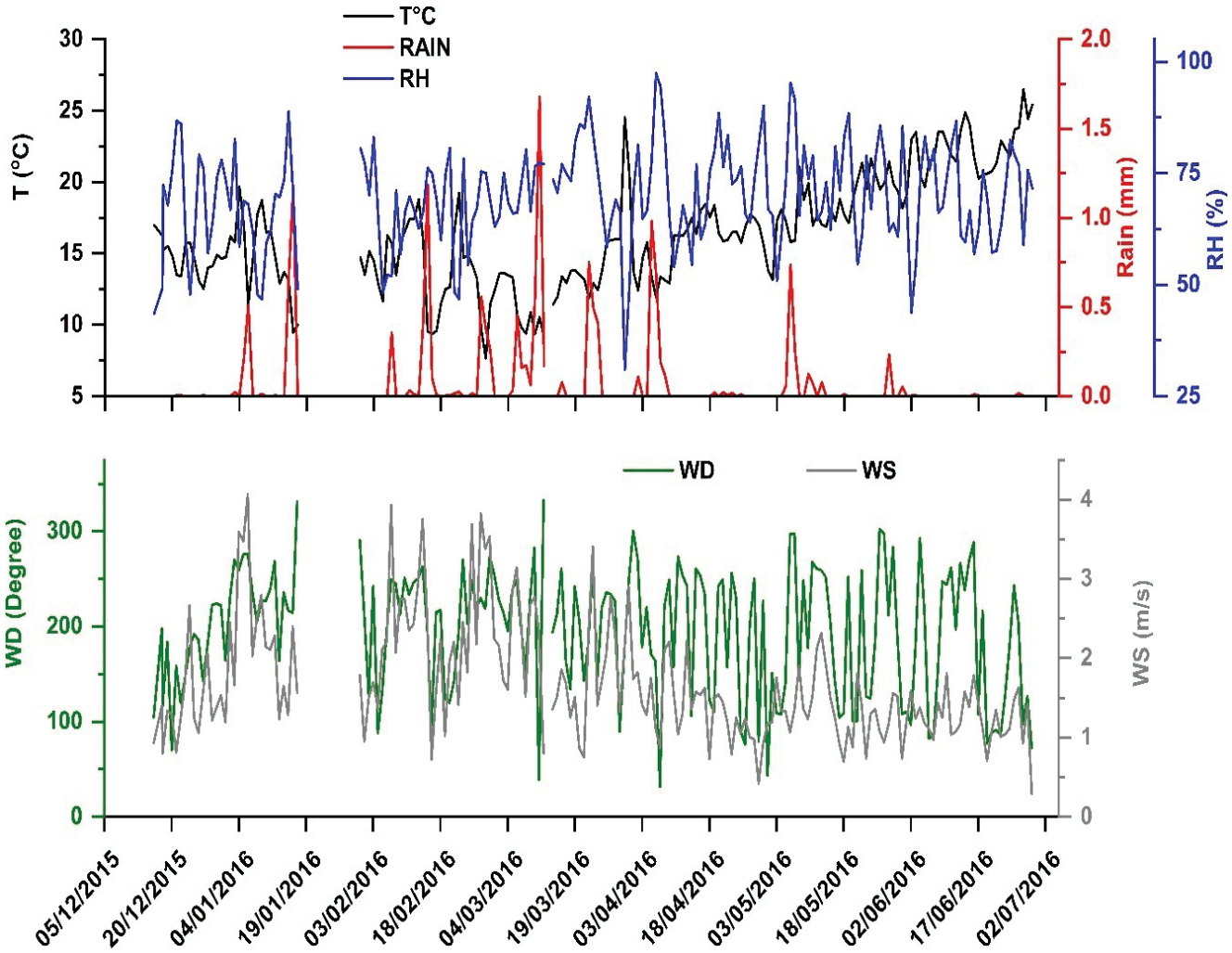

Figure 1: *Meteorological parameters (Wind speed, Wind direction, Temperature, Rain, and Humidity) at Boulsmaïl station.*

Figure 2 represents the four significant periods during the campaign. The first time (December 16-17, 2015) coincides with air masses originating from the Atlantic Ocean, across Portugal and southern Spain, and reaching the Mediterranean Sea. The second phase (December 21-22, 2015) is characterised by the influx of air masses from the Mediterranean Sea, traversing western Algeria. The third phase, from February 21 to 22, 2016, is characterised by the influx of air masses originating from Mauritania and traversing through Mali, then crossing Algeria's southern region.

The last phase (February 22-23, 2016) is characterised by air masses originating from eastern Algiers and moving over the Mediterranean Sea. The main focus of the public now is the decrease in air quality and how it affects both the environment and human health. The most notable clusters originate from

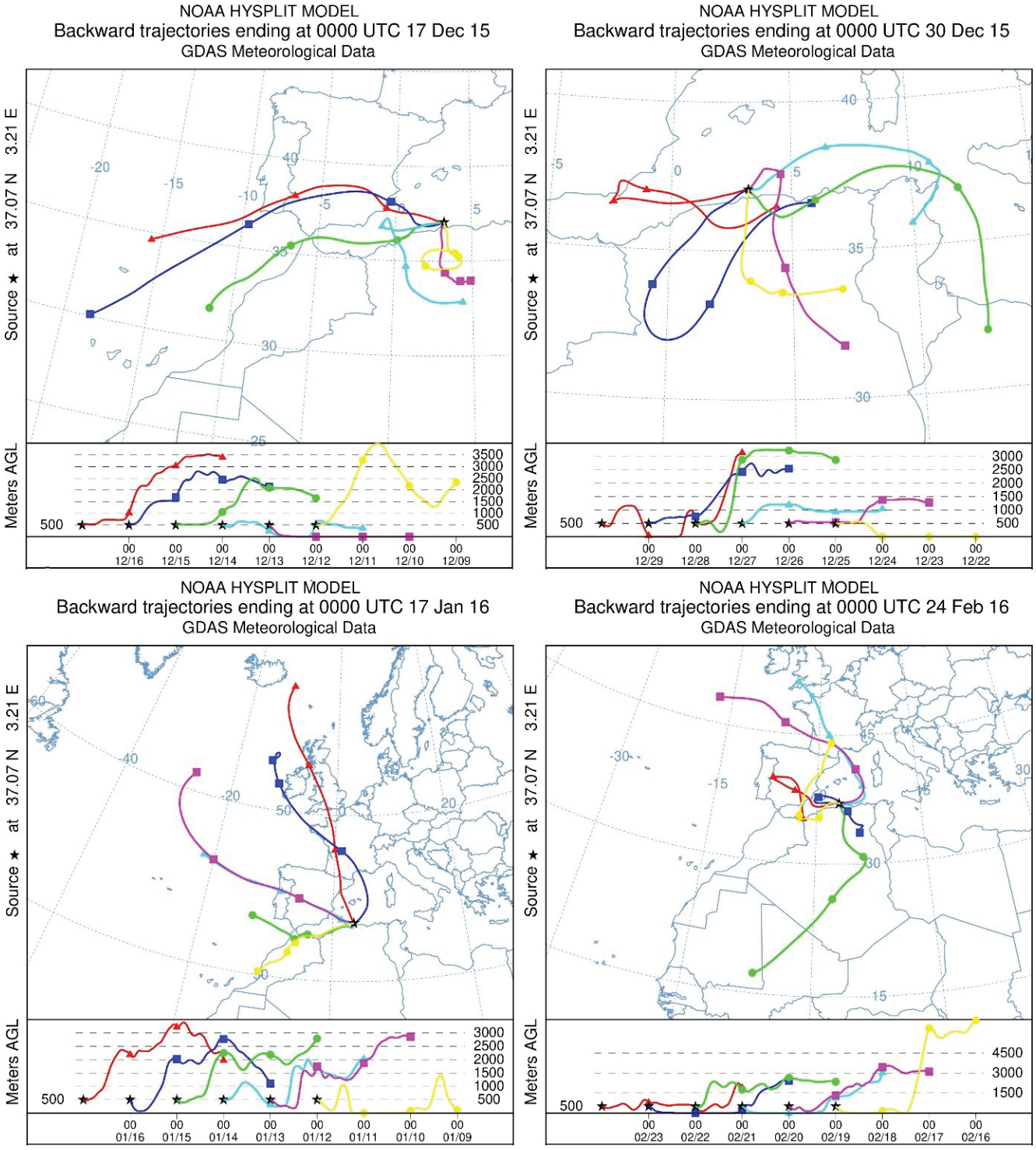

Figure 2: *Mean back-trajectories arriving at Bou-Ismail station.*

Table 1: *Seasonal variations of contaminants and climatic conditions during the measurement campaign.*

	Winter (From December 15 to March 31, 2016)													
	NO	**NO_2**	**CO**	**O_3**	**SO_2**	**VOC**	**PM_{10}**	**$PM_{2.5}$**	**T**	**P**	**RAIN**	**RH**	**WD**	**WS**
	ppb	ppb	ppm	ppb	ppb	ppm	µg/m³	µg/m³	°C	hPa	mm	%	Degree	m/s
Average	6.4	12.9	0.0	23.8	0.3	0.0	29.2	13.4	14.0	1000.2	0.1	68.1	205.2	2.0
Mean standard error	0.4	0.7	0.0	0.8	0.1	0.0	2.1	1.0	0.3	0.8	0.0	1.2	5.8	0.1
Median	5.3	11.1	0.0	24.4	0.0	0.0	21.9	10.4	13.8	1000.4	0.0	69.1	216.9	2.0
Standard deviation	3.4	6.6	0.2	7.3	0.6	0.0	20.6	9.7	2.8	7.6	0.3	11.6	56.4	0.8
Minimum	0.7	3.1	0.0	9.0	0.0	0.0	4.1	2.3	7.7	981.4	0.0	31.0	38.9	0.7
Maximum	20.9	34.1	1.5	39.7	3.5	0.1	116.0	47.7	24.5	1013.4	1.7	92.0	332.8	4.1
25th percentile	4.2	8.3	0.0	19.5	0.0	0.0	15.6	6.4	12.5	995.4	0.0	62.2	171.1	1.4
50th percentile	5.3	11.1	0.0	24.4	0.0	0.0	21.9	10.4	13.8	1000.4	0.0	69.1	216.9	2.0
75th percentile	**7.6**	**15.9**	**0.0**	**29.2**	**0.2**	**0.1**	**39.6**	**17.9**	**15.8**	**1006.4**	**0.0**	**75.7**	**242.2**	**2.5**
	Spring (From April 1, 2016, to June 29, 2016)													
	NO	**NO_2**	**CO**	**O_3**	**SO_2**	**VOC**	**PM_{10}**	**$PM_{2.5}$**	**T**	**P**	**RAIN**	**RH**	**WD**	**WS**
	ppb	ppb	ppm	ppb	ppb	ppm	µg/m³	µg/m³	°C	hPa	mm	%	Degree	m/s
Average	4.8	11.2	0.5	28.1	0.0	0.1	10.8	4.2	18.8	995.3	0.0	71.6	185.4	1.3
Mean standard error	0.2	0.4	0.1	0.5	0.0	0.0	0.7	0.3	0.4	0.6	0.0	1.2	7.9	0.0
Median	4.8	10.6	0.5	28.2	0.0	0.1	8.3	3.2	18.4	995.6	0.0	71.8	192.2	1.3
Standard deviation	1.5	3.5	0.5	4.7	0.1	0.0	6.6	2.7	3.3	5.4	0.2	10.9	74.4	0.4
Minimum	1.7	5.3	0.0	11.9	0.0	0.0	2.9	0.6	11.9	960.6	0.0	43.7	31.8	0.3
Maximum	8.5	20.0	1.5	38.2	0.4	0.2	33.2	12.2	26.5	1004.7	1.0	97.4	302.1	2.3
25th percentile	3.8	8.6	0.0	25.4	0.0	0.1	6.3	2.0	16.5	993.1	0.0	63.6	109.3	1.1
50th percentile	4.8	10.6	0.5	28.2	0.0	0.1	8.3	3.2	18.4	995.6	0.0	71.8	192.2	1.3
75th percentile	**5.8**	**12.8**	**1.0**	**31.5**	**0.0**	**0.1**	**15.3**	**6.1**	**21.4**	**998.4**	**0.0**	**79.1**	**251.5**	**1.5**

T: Temperature, P: Pressure, RH: Relative humidity, WS: Wind speed, WD: Wind direction

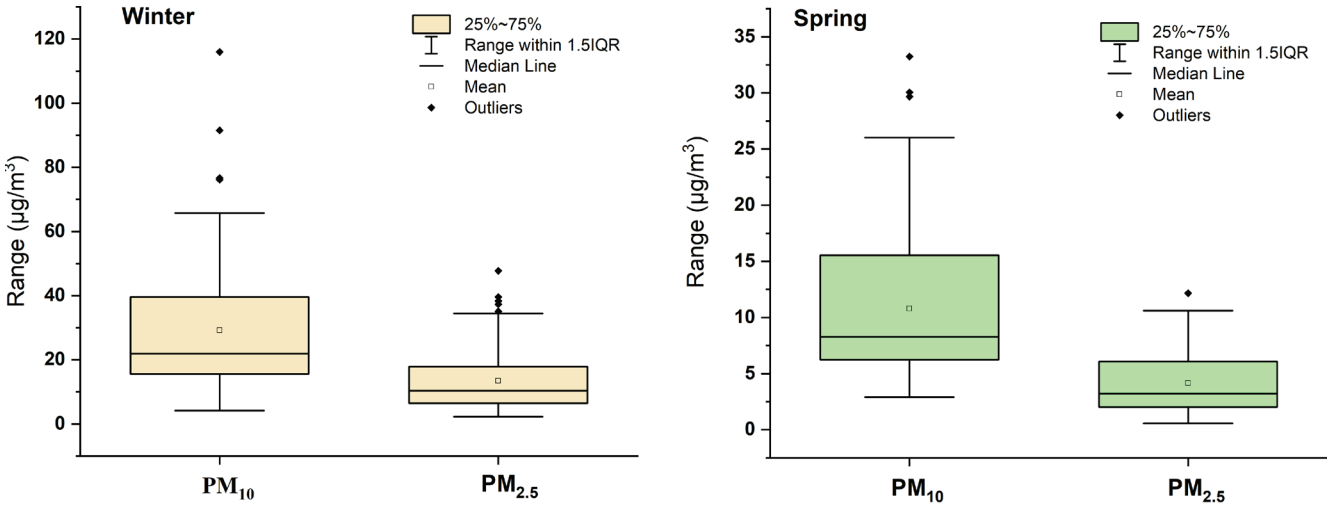

Figure 3: *Plots of two PMs (µg/m³) in a box and whisker distribution. The boxes' bottom border symbolises the 25th percentile, the middle line the 50th percentile, and the top square the 75th percentile. The whiskers represent the lowest and maximum.*

major industrial locations and those most affected by vehicle emissions.

Table 1 displays the measurement campaign's seasonal variation of pollutants and meteorological conditions (Supplementary material, Table S3, including monthly concentrations of $PM_{2.5}$, PM_{10}, and gaseous pollutants measured during the sampling campaign). The average concentrations of PM_{10}, $PM_{2.5}$, VOCs, SO_2, NO_2, and NO all parameters decreased from winter to spring, but CO increased from 0.0 ppm in winter to 0.5 ppm in spring, O_3 raised by 18 percent (from 23.8 ppb to 28.1 ppb), and VOCs elevated from below the detection limit to an average of 0.1 ppm (Supplementary Figure S2, presenting box and whisker plots of NO, NO_2, and O_3 concentrations across the sampling period). Figure S2 illustrates the mean diurnal patterns of major pollutants and particulate matter at the Bou-Ismail site. NO and NO_2 exhibit bimodal maxima during morning (approximately 07:00–09:00 local time) and evening (around 17:00–19:00 local time) traffic congestion, with levels declining to minima overnight. CO exhibits relative constancy throughout the day, with a slight increase around noon, indicative of consistent background emissions and diminished removal activities. O_3 concentrations rise post-sunrise, peaking in the early afternoon (approximately 13:00–15:00 local time) due to heightened photochemical reactions, before declining in the evening. PM_{10} and $PM_{2.5}$ exhibits a midday peak aligned with atmospheric mixing and afternoon emissions, whereas concentrations are reduced throughout the night and early morning. These patterns indicate that transportation is the primary contributor to NO_x and PM peaks, whereas photochemistry is responsible for the afternoon O_3 maximum. Previous investigations have shown that the release of O_3 precursors, including NO_x, CO, and VOCs, varies between weekdays and weekends due to differences in traffic and industrial operations (Cai et al. 2019; Zhang et al. 2023).

According to the data collected from the monitoring station, the average concentration of $PM_{2.5}$ in winter was 13.4 µg/m³, whereas in spring, it was 4.2 µg/m³ (Table 1).

The highest and lowest daily PM_{10} concentration values recorded during the winter and spring seasons were 116.0 µg/m³ and 4.1 µg/m³, and 33.2 µg/m³ and 2.9 µg/m³, respectively. The mean concentrations of PM_{10} throughout the winter and spring seasons, based on the data collected from the monitoring station, were 29.2 µg/m³ and 10.8 µg/m³, respectively, as seen in Figure 3.

Figure 3 illustrates box plots that depict the distribution of daily concentrations of PM_{10} and $PM_{2.5}$ across the winter and spring. During the winter season, PM_{10} concentrations exhibit a higher median of approximately 20 µg/m³ and a broader interquartile range, with the upper whisker extending to approximately 65 µg/m³. Multiple outliers exceed 80 µg/m³, with the absolute maximum concentration reaching 116.0 µg/m³ (as shown in Table 1), indicating severe pollution episodes during the winter

Table 2: *Seasonal $PM_{2.5}$ and PM_{10} Concentrations in Bou-Ismail and Comparative Mediterranean and North African Sites*

Season	Location	$PM_{2.5}$ (µg/m³)	PM_{10} (µg/m³)	Reference
Winter	Bou-Ismail, Algiers	13.4	29.2	Present study
Winter	Meknes city, Morocco	25.8	35.1	(Ait Bouh et al. 2023)
Winter	Kenitra, Morocco	17.1	40.2	(Bounakhla et al. 2023)
Winter	Tetouan city, Northern Morocco	21.0	32.3	(Benchrif et al. 2025)
Winter	Montseny, Spain	9	12	(Cusack et al. 2013)
Winter	Finokalia, Greece	8	14	(Querol et al. 2009)
Winter	Naples, Italy	28	37	(Di Vaio et al. 2016)
Winter	Salentum peninsula, Italy	15	24	(Contini et al. 2014)
Winter	Anatolie, Turkey	45	71	(Tayanç et al. 2022)
Winter	Erdemli, Turkey	14	24	(Querol et al. 2009)
Spring	Bou-Ismail, Algiers	4.2	10.8	Present study
Spring	Meknes city, Morocco	23.4	39.2	(Ait Bouh et al. 2023)
Spring	Kenitra, Morocco	16.1	44.1	(Bounakhla et al. 2023)
Spring	Tetouan city, Northern Morocco	15.8	29.1	(Benchrif et al. 2025)
Spring	Tetouan city, Northern Morocco	15.8	29.1	(Benchrif et al. 2025)
Spring	Montseny, Spain	12	15	(Cusack et al. 2013)
Spring	Finokalia, Greece	13	19	(Querol et al. 2009)
Spring	Naples, Italy	22	29	(Di Vaio et al. 2016)
Spring	Salentum peninsula, Italy	19	31	(Contini et al. 2014)
Spring	Anatolie, Turkey	32	54	(Tayanç et al. 2022)
Spring	Erdemli, Turkey	18	41	(Querol et al. 2009)

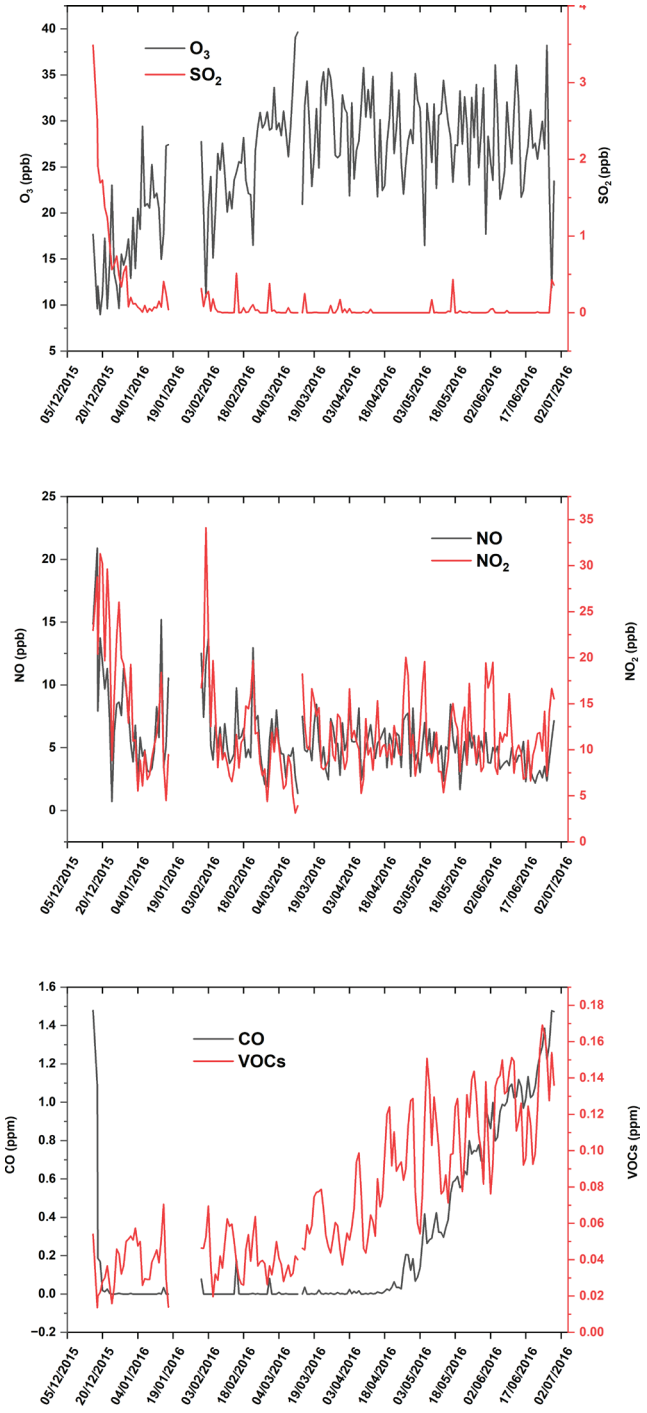

Figure 4: *Hourly average concentration time series for gases.*

period. $PM_{2.5}$ concentrations exhibit a median of approximately 15 µg/m³, accompanied by a broader distribution in comparison to spring. The outliers approach 40 µg/m³. During the spring season, levels of both PM_{10} and $PM_{2.5}$ are markedly reduced. The median concentration of PM_{10} is approximately 7 µg/m³, while $PM_{2.5}$ is marginally lower at around 5 µg/m³. The interquartile ranges are narrower, and the occurrence of outliers is diminished, suggesting more stable air quality conditions. This figure illustrates a distinct seasonal trend, characterised by elevated levels and increased variability in particulate matter during the winter. This phenomenon is likely attributable to diminished atmospheric dispersion, heightened heating activities, and the potential impact of long-range transported dust or pollution. In contrast, spring demonstrates superior air quality and more stable values (Bounakhla et al. 2023; Amare et al. 2024; Bamola et al. 2024). The box plot analysis reveals that while most winter PM_{10} concentrations fell within the interquartile range, the presence of multiple outliers above 80 µg/m³, including the absolute maximum of 116.0 µg/m³, demonstrates the occurrence of significant pollution episodes that substantially exceeded typical winter levels.

The analysis reveals that Bou-Ismail exhibits moderate PM concentrations compared to other Mediterranean sites (Table 2). During winter, $PM_{2.5}$ levels are recorded at 13.4 µg/m³, which is lower than the levels found in Crete, Kenitra, and northwestern Morocco, yet higher than those in rural areas such as Pontokomi. Spring concentrations indicate a significant decrease in Bou-Ismail ($PM_{2.5}$: 4.2 µg/m³; PM_{10}: 10.8 µg/m³), which are considerably lower than those in most other locations for comparison. The seasonal variation pattern observed in Bou-Ismail aligns with the broader Mediterranean trend of higher concentrations in winter, followed by decreases in spring (Querol et al. 2004; Grivas and Chaloulakou 2006; Bounakhla et al. 2023). The results correspond with the wider Mediterranean trend noted in Southern Italy (e.g., Lecce), where both PM fractions show elevated concentrations in winter, followed by a decline in spring, although specific seasonal averages were not included. The concentrations observed in Bou-Ismail suggest that particulate matter levels are relatively lower compared to those in various urban and semi-urban locations throughout the Mediterranean and North Africa, especially in the spring season. The observed differences probably indicate a mix of local emission sources, variations in meteorological conditions, and topographical influences (Querol et al. 2004; Grivas and Chaloulakou 2006; Bounakhla et al. 2023). There were five prominent pollution events when the concentration of PM_{10} exceeded 80 µg/m³. Significant pollution levels were seen from February 22 to February 23, with PM_{10} concentrations above 91 mg/m³.

Figure 4 shows the variability in the average hourly levels of pollutants over the days seen in the sample period. Our analysis reveals that the average hourly concentrations of NO and NO_2 show consistent stability at low levels from midnight until seven in the morning. Elevated concentrations of NO and NO_2 are observed between 07:00 and 18:00. This pattern reflects the presence of a shallow nocturnal boundary layer that traps emissions near the surface, followed by boundary-layer growth after sunrise, which enhances vertical mixing and promotes the photochemical oxidation of NO and NO_2 (Wikuats et al. 2023). Nitrogen oxides are formed by the oxidation of atmospheric nitrogen in high-temperature combustion operations, which include transportation, home heating, energy generation, and some chemical industrial activities. The high levels of NO and NO_2 detected at the sample location are due to its proximity to the Bou-Ismail industrial zone and the heavily trafficked national route of Bou-Ismail-Blida, which houses chemical

manufacturing facilities. The concentration of NO rose at 9 a.m. and reached its maximum at 6 p.m. (11 ppb), going down after 7 p.m., while the minimum concentration was seen between 3 a.m. and 7 a.m. (1 ppb). For NO_2, the highest concentration was 18 ppm at 9 p.m., while the lowest was 9 ppm at 6 a.m. Due to road traffic, the mean hourly concentrations of SO_2 show prominent peaks during the morning (0.1, 0.4 ppb) and the evening peak hours (0.1, 0.11 ppb). SO_2 is released into the atmosphere via both human-made and natural sources. It has been calculated that over 70% of worldwide SO_2 emissions originate from human-made sources, with fossil fuel burning being the main contributor (Singh and Tripathi 2021). More sources of SO_2 include biomass burning, shipping, metal smelting, agricultural waste burning, the pulp and paper industry, and a small volcanic contribution. SO_2 gas is well-acknowledged to induce irritation in the respiratory tract and the mucous membranes of the skin and eyes, potentially leading to asthma (De Ferreyro Monticelli et al. 2021). SO_2 levels declined from a winter average of 0.30 ppb to 0.04 ppb in spring—a 7.5-fold reduction—primarily due to reduced household heating and the prevalence of calmer marine airflows (Table 1), consistent with seasonal patterns reported for north-western Morocco (Bounakhla et al. 2023).

O_3 concentrations showed a modest increase relative to the levels observed between 00:00 and 08:00 (Supplementary material, Figure S3, depicting mean hourly concentration profiles for PM and gaseous pollutants at the Bou-Ismail station). O_3 is a secondary pollutant produced in the atmosphere via intricate, non-linear, and temperature-dependent photochemical processes involving VOC and NO_x (Pusede et al. 2015; Ma et al. 2019).

CO concentration was stable over 24 hours (Supplementary material, Figure S2, depicting mean hourly concentration profiles for PM and gaseous pollutants at the Bou-Ismail station), with a slightly elevated concentration at 11 a.m. (0.31 ppm). High concentrations were seen between 2 p.m. and 7 p.m. (~ 33 ppb). An increase was seen for SO_2 from 11 a.m. (the highest value was 0.19 ppb). Average VOC concentrations are more stable during the day (~ 0,1 ppm) (Supplementary material, Figure S4, showing seasonal box and whisker distributions of VOC concentrations during winter and spring).

Both NO and NO_2 showed a clear diurnal pattern, rapidly going up from late morning and peaking in the afternoon. The highest CO, SO_2, and PM_{10} levels were recorded during the morning rush hour, which went down in the late morning because of the rapid expansion of the planetary boundary layer and reduced emissions. A secondary peak was seen with lower levels during the evening rush hour, likely due to decreased human activities. The weekend impact for these compounds is clear (Supplementary material, Figure S2, depicting mean hourly concentration profiles for PM and gaseous pollutants at the Bou-Ismail station), showing reduced morning peaks on Friday and Saturday compared to the weekdays (Sunday to Thursday). The noticeable rises in CO and PM_{10} levels on Friday, Saturday, and Sunday nights persisted into the early hours of the next day, likely due to heightened human activity during weekend evenings.

However, out of the 196 days of the monitoring period, $PM_{2.5}$ and PM_{10} levels exceeded the 2021 World Health Organization (WHO) Air Quality Guidelines (AQG), which were 15 and 45 µg/m³ for a duration of 24 hours, respectively on 27 (14.7%) and 17 (9.2%) days, mainly during the winter months (December to March).

For NO_2, only 3.3% of the data exceeded the AQG reported by WHO for the 24-hour mean, but it was not exceeded for the 1-hour mean (concentration up to 200 µg/m³, not shown). The levels of SO_2 and CO in Bou-Ismail were far below the WHO/AQG thresholds, as seen in the graphs. During the monitoring period, there has been a significant decrease in SO_2 levels in Bou-Ismail because of the reduced sulfur content in vehicles and industrial fuels. The WHO 2021 AQGs represent a revolutionary strengthening of air quality protection, with most limits reduced by 25-75% based on compelling new health evidence showing adverse effects at all exposure levels. Algerian air quality rules (Decree 06-02/2006) (OJRA 2006), which is dramatically less protective than the 2021 WHO Air Quality Guidelines released on September 22, 2021. Algeria's SO_2 limit of 125 µg/m³ (48 ppb) for 24 hours is 3.1 times higher than the WHO 2021 guideline of 40 µg/m³ (15 ppb), while NO_2 standards are 8 times higher than the WHO recommendations (WHO 2021).

Therefore, it is critically urgent to monitor the levels of air pollutants and implement comprehensive regulatory reform aligning with the WHO 2021 guidelines to eliminate the massive protection gap and prevent thousands of preventable deaths annually, to enforce stricter laws that meet the WHO criteria to reduce the present delay.

Relationships between variables: correlation analysis

The current study used Pearson correlation analysis to determine the association between various air contaminants, to identify site-specific emission source signatures, and assess how local meteorological conditions influence pollutant co-variation patterns in this understudied North African urban environment. We expected to gain new insights into the impact of Saharan dust intrusions on $PM_{2.5}$–PM_{10} relationships and the seasonal modulation of secondary organic aerosol formation under hot, arid conditions. While general pollutant relationships are established, this analysis aimed to detect unique source contributions (e.g., Saharan dust influence, regional biomass burning patterns) and secondary formation processes that differ from well-characterized European and North American urban areas.

Table 3 shows the Pearson correlation coefficients (p-value <0.01) for daily pollutant concentrations over the full monitoring period. Meteorological conditions significantly affect air quality (Zhang et al. 2018; Xiao et al. 2020). Hence, their impacts should be considered when assessing the influence of pollution sources. We utilized meteorological data (pressure, temperature, wind

speed, wind direction, relative humidity, and precipitation), air quality data ($PM_{2.5}$, PM_{10}, CO, SO_2, NO, NO_2, O_3), and data from continuous tracking systems from the viewpoint of big data statistics. Because our six-month campaign covers only winter and spring, interpretations of linear correlations must be made with caution, particularly for inherently non-linear processes such as NO_x–O_3 photochemistry. We therefore highlight the most robust site-specific relationships, notably $PM_{2.5}$–PM_{10} clustering and indications of common NO–NO_2–SO_2 sources.

SO_2 and NO_2 undergo atmospheric oxidation processes that lead to the formation of secondary inorganic aerosols, such as sulfates and nitrates, which are key components of particulate matter (Ma et al. 2019). The results showed correlations between NO,

Table 3: *Pearson correlation coefficients between PM_{10}, $PM_{2.5}$, and gas pollutants concentrations, and weather in Bou-Ismail station.*

	NO	NO_2	CO	O_3	SO_2	VOCs	PM_{10}	$PM_{2.5}$	T	P	RAIN	RH	WD	WS
NO	—													
NO_2	0.69 [c]	—												
CO	-0.12	0.05	—											
O_3	-0.52 [c]	-0.72 [c]	0.06	—										
SO_2	0.60 [c]	0.58 [c]	0.10	-0.52 [c]	—									
VOCs	-0.26	-0.11	0.74 [c]	0.24 [c]	-0.28 [c]	—								
PM_{10}	0.61 [c]	0.61 [c]	-0.23 [b]	-0.61 [c]	0.49 [c]	-0.44 [c]	—							
$PM_{2.5}$	0.63 [c]	0.72 [c]	-0.22 [b]	-0.68 [c]	0.63 [c]	-0.41 [c]	0.91 [c]	—						
T	-0.19 [a]	0.04	0.77 [c]	0.01	-0.08	0.71 [c]	-0.21 [b]	-0.25 [c]	—					
P	0.40	0.50 [c]	-0.05	-0.47 [c]	0.43 [c]	-0.30 [c]	0.57 [c]	0.60 [c]	-0.11	—				
RAIN	-0.11	-0.28 [c]	-0.18 [a]	0.18 [a]	-0.04	-0.13	-0.14	-0.11	-0.39 [c]	-0.28 [c]	—			
RH	0.02	-0.05	-0.02	0.10	-0.13	0.42 [c]	-0.20 [b]	0.01	-0.23 [b]	-0.16 [a]	0.25 [c]	—		
WD	0.06	-0.32 [c]	-0.21 [b]	0.26 [c]	-0.18 [a]	-0.12	-0.05	-0.12	-0.14	-0.16 [a]	0.02	0.04	—	
WS	-0.17 [a]	-0.35 [c]	-0.40 [c]	0.11	-0.14	-0.51 [c]	0.04	-0.05	-0.31 [c]	-0.20 [b]	0.31 [c]	-0.30 [c]	0.42 [c]	—

a Correlation is significant at the 0.05 level.
b Correlation is significant at the 0.01 level.
c Correlation is significant at the 0.001 level.
T: Temperature, P: Pressure; RH: Relative humidity, WS: wind speed

Table 4: *Principal component analysis factor for the Bou-Ismail site sample*

	Principal component analysis			
Compounds	**Traffic-related pollutants**	**Volatile compounds**	**Humidity factor**	**Wind influence**
NO	0.81	-0.04	0.18	0.23
NO_2	0.87	0.17	0.06	-0.17
CO	-0.09	0.84	0.05	-0.16
O_3	-0.78	-0.01	0.09	0.18
SO_2	0.73	-0.01	-0.02	-0.14
VOCs	-0.33	0.79	0.45	-0.06
PM_{10}	0.84	-0.19	-0.17	0.08
$PM_{2.5}$	0.91	-0.20	0.02	0.00
T (Temperature)	-0.13	0.90	-0.20	-0.04
P (Pression)	0.69	0.00	-0.18	-0.10
RAIN	-0.27	-0.56	0.34	-0.20
RH (Relative humidity)	-0.07	-0.05	0.94	0.05
WD (Wind direction)	-0.15	-0.13	0.01	0.94
WS (Wind speed)	-0.23	-0.56	-0.44	0.36
Eigen values	4.83	2.90	1.55	1.24
% of Total Variance	34.53	20.74	11.07	8.88
Cumulative contribution	24.53	55.27	66.34	75.22

Note: extraction method based on principal component analysis with varimax rotation; a bold is main load (>0.5).

NO_2, and SO_2 (between 0.58 and 0.69), suggesting that industrial sources and the combustion of sulfur-containing fossil fuels are likely to contribute to this pollutant. But correlations were seen between NO, NO_2, $PM_{2.5}$, PM_{10} and SO_2, suggesting that these pollutants probably originate from the same source, i.e. the exhaust from vehicles running on gasoline and sulfur-containing fuels. CO may represent the effects of mixing and dilution on pollution levels (Ma et al. 2019). CO correlates positively with O_3 and VOCs. Another strong association was found between ozone and temperature, supporting the photochemical production mechanism of ozone (Pusede et al. 2015; Li et al. 2021). While the general O_3-relationship is well established, our findings quantitatively confirm its strength under local conditions—specifically, an r-value notably higher than those reported for inland Mediterranean sites—highlighting the amplified temperature sensitivity of O_3 formation in this urban coastal environment. However, NO, NO_2, SO_2, and O_3 have not shown correlations with Rain, WS, and RH, respectively. The association between O_3, NO, and NO_2 was somewhat negative, suggesting the significance of NO and NO_2 in the depletion of O_3. Particles may hinder the passage of light, which is not favourable for O_3 production. No correlation was seen between these species. No association between O_3, NO, and NO_2 suggests that O_3 generation could occur in the VOC-limited regime. No significant correlation was seen between pollutants and Relative humidity and wind speed. A strong correlation has been found between $PM_{2.5}$ and PM_{10}. The high association between $PM_{2.5}$ and PM_{10} suggests that they likely originate from the same emission sources (Zhou et al. 2016; Bamola et al. 2024). $PM_{2.5}$ and PM_{10} show no relationship with meteorological conditions, implying that particle levels are associated with tranquil conditions marked by low wind speeds and cold temperatures.

Principal component analysis

Principal component analysis (PCA) was used to examine the variability patterns in this multivariate dataset. PCA was used to investigate the variability patterns in this multivariate dataset, identify the dominant pollutant source factors (e.g., traffic emissions, VOC sources, meteorological influences), and quantify their relative contributions to air quality variability in Bou-Ismail. A PCA model was created for air pollutants (CO, NO, NO_2, SO_2, PM_{10}, and $PM_{2.5}$) and meteorological variables (Pressure, rain, temperature, relative humidity, wind direction, and wind speed). Table 4 displays the PCA loadings acquired for the sampling periods in the full monitoring period. PCA was used to examine the variability patterns in this multivariate dataset. Table 4 presents the principal component analysis obtained for the sample periods using the full monitoring period.

Principal components with eigenvalues greater than 1 were kept under the Kaiser criteria (Supplementary material, Tables S4 and S5, showing PCA eigenvalues and validation results from KMO and Bartlett's tests). The PCA yielded four components, accounting for about 75.22% of the overall variation (Supplementary material, Table S4, which provides eigenvalues and percentage variances explained by each principal component in the PCA). A fourth potential element was examined in Bou-Ismail. No precise physical or source-related process could be linked to the fourth principal component; hence, only three components were kept. Loadings greater than 0.5 are considered strong; those between 0.2 and 0.5 are moderate, and those less than 0.2 are weak, for the discussion (Table 4). Principal Component 1 (PC1) explained a significant part (35.38%) of the overall variance (Supplementary material, Table S4, which provides eigenvalues and percentage variances explained by each principal component in the PCA, and Figure S5, which displays PCA biplots for pollutant and meteorological data), significant loadings for particulate and some gases (Table 4), with a minor contribution of VOCs. This suggests that transportation emissions are the primary source of air pollution in the area. PC2 accounted for 21.75%, a significant contribution of CO and VOCs. The primary industries generating VOCs are building, followed by transport and agriculture. Car traffic is the primary source of CO. The source attributions correspond with the real-time measuring capabilities of the Airpointer monitoring system, which distinguishes between traffic-related pollutants, VOC emissions, and other gaseous species via its integrated sensor array. PC3 (10.71%) shows strong contributions from relative humidity (RH), implying meteorological influences on pollutant dispersion and transformation.

PC4 (7.38%) is primarily influenced by wind direction and speed, reflecting the impact of regional transport dynamics on pollutant variability.

Hierarchical cluster analysis

We used hierarchical cluster analysis (HCA) to find reasonably homogeneous data group of pollutants and meteorological variables that behave similarly, in order to elucidate underlying source categories and environmental factors influencing air quality variability in Bou-Ismail. The items inside the same cluster show similarity according to the established selection criteria. A cluster analysis was conducted using Ward's approach, utilising Euclidean distances as the criteria for cluster formation. Although this HCA is highly efficient, it often results in small clusters (Shrestha and Solomatine 2006). Due to significant disparities in scale among the variables, standardisation was performed before computation (Supplementary material, Figure S6, presenting the dendrogram from hierarchical clustering of air quality parameters), and it exhibits four clusters: (C1) NO-NO_2-SO_2; (C2) PM_{10}-$PM_{2.5}$-P; (C3) CO-T -VOC; and (C4) O_3-WD -WS -RAIN-RH.

These clusters represent significant groupings that are aligned with the physical and chemical properties of the contaminants and meteorological circumstances. Comparable clustering tendencies have been documented in the literature. Because they all originate from the same places—i.e., transportation and combustion NO, NO_2, and SO_2 tend to mix (Grivas and Chaloulakou 2006). This finding aligns with previous work reporting comparable PM-meteorology clustering in Seoul, Korea (Seo et al. 2018), thereby demonstrating the role of atmospheric stability in shaping PM dynamics across

metropolitan environments. Furthermore, VOC and CO clustered with temperature, showing their photochemical interactions and emission properties (Munir et al. 2013). Ultimately, O_3 frequently correlated with relative humidity, wind speed, and solar radiation in several investigations, corroborating its secondary generation and environmental reliance (Han et al. 2020).

Integrated Multivariate Analysis of Air Quality Drivers in Bou-Ismail

This section begins with a summary statement that integrates all multivariate findings.

Multivariate analyses indicate that local traffic and combustion emissions are the primary factors influencing air quality variability in Bou-Ismail, whereas relative humidity and wind patterns regulate pollutant dispersion and secondary formation.

The PCA results are presented, followed by HCA groupings and significant R correlations. Each component and cluster are cross-referenced to demonstrate their convergence on the same source attributions, such as the alignment of PC1 loadings of $PM_{2.5}$, NO, NO_2, and SO_2 with HCA Cluster 1 and the strong R correlations among these species. We examine the humidity-related PCA component (PC3) and its associated cluster, which elucidate the observed negative correlation between relative humidity and particulate concentrations. Additionally, PC4, representing wind influence, along with the O_3 meteorology cluster, underscores the effects of regional transport. This integrated presentation elucidates the primary conclusion that traffic emissions are the predominant source of primary pollutant levels, while meteorological factors influence their ambient concentrations and secondary formation.

Air Quality Index (AQI) at Bou-Ismail and Its Comparison with Other Studies

AQI was determined by using the recorded daily $PM_{2.5}$ and PM_{10} concentrations. The air quality indices calculated each day for the two fractions, PM_{10} and $PM_{2.5}$, in our study are presented in Table 5 and Figure 5. So, the heightened AQI values seen in this research indicate higher concentrations of ambient PM in Bou-Ismail. This also results in significant serious health hazards for the exposed population. For $PM_{2.5}$ and PM_{10}, the study's average AQI was 40 and 18.3, respectively.

Throughout the study period, the AQI for SO_2, NO_2, and CO consistently remained in the “Good” category, confirming that their ambient concentrations were well below both WHO guideline values and Algerian standards. Eight-hour O_3 levels also fell within the “Good” category, suggesting minimal photochemical smog formation during the observation period. The one-hour O_3 sub-index was classified as “Good” for 99.74%

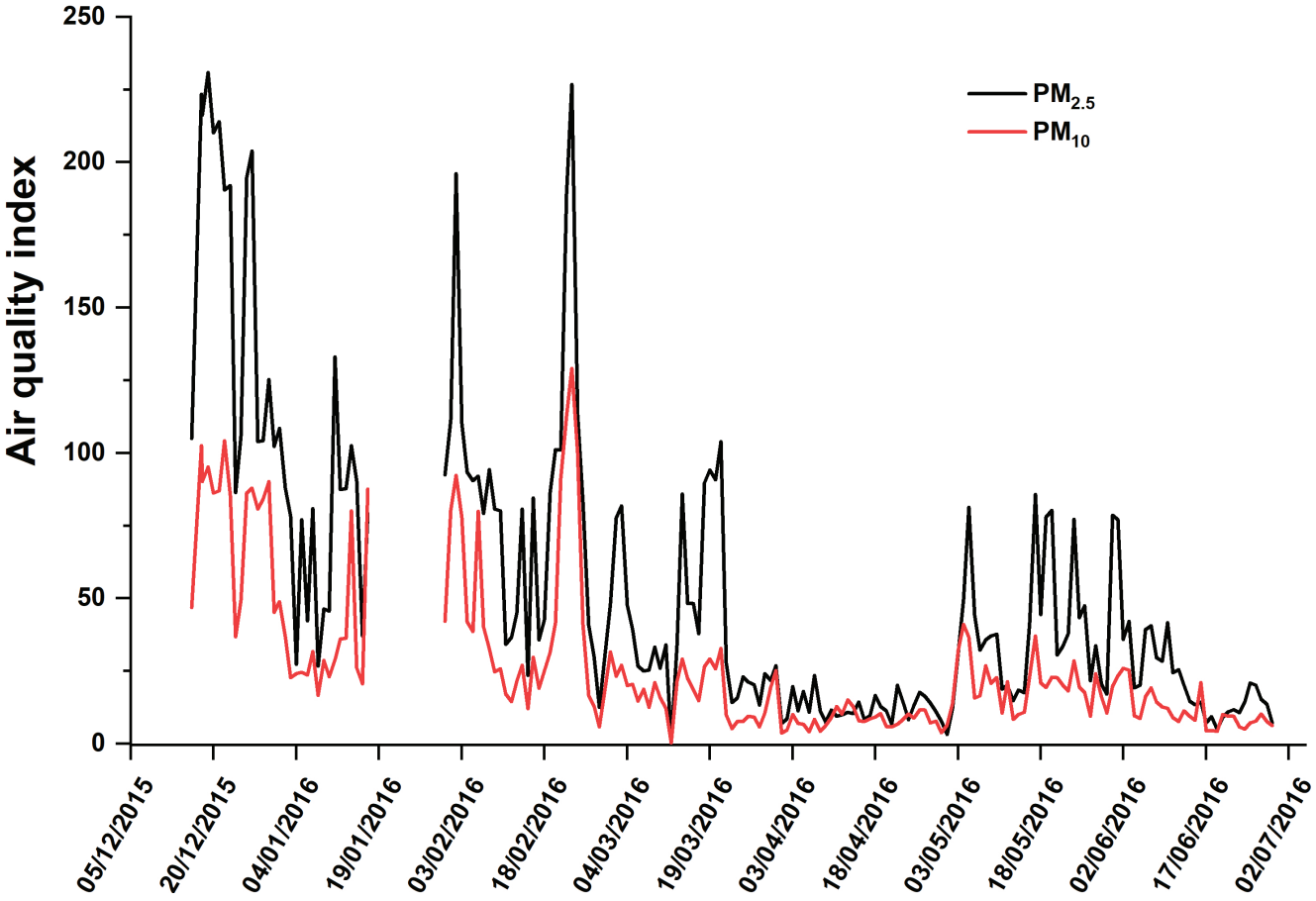

Figure 5: *The $PM_{2.5}$ and PM_{10} Air Quality Index, measured in Bou-Ismail, are shown as bar graphs. The U.S. Environmental Protection Agency (EPA) guidelines are the basis for AQI calculations.*

Table 5: *Contribution (%) of air quality index for Bou-Ismail station.*

Components	$PM_{2.5}$	PM_{10}	SO_2	NO_2	CO	O_3	O_3
Times (average)	24h	24h	8h	8h	1h	8h	1h
Good	77.0	94.6	100	100	100	100	99.74
Moderate	15.8	5.4	0.0	0.0	0.0	0.0	0.26
Unhealthy for sensitive groups	5.5	0.0	0.0	0.0	0.0	0.0	0.0
Unhealthy	1.1	0.0	0.0	0.0	0.0	0.0	0.0
Very unhealthy	0.5	0.0	0.0	0.0	0.0	0.0	0.0
Hazardous	0.0	0.0	0.0	0.0	0.0	0.0	0.0

Table 6: *Estimated HQ values of $PM_{2.5}$ and PM_{10} at different monitoring periods at Bou-Ismail station.*

		December	January	February	March	April	May	June	Total
$PM_{2.5}$	Average	1.86	0.71	0.90	0.47	0.15	0.42	0.26	0.59
	Min	0.83	0.32	0.15	0.16	0.08	0.04	0.06	0.04
	Max	3.86	1.34	2.55	1.23	0.28	0.81	0.61	3.18
PM_{10}	Average	1.03	0.52	0.67	0.29	0.13	0.33	0.18	0.40
	Min	0.60	0.27	0.09	0.08	0.06	0.10	0.07	0.06
	Max	1.53	1.08	2.32	0.53	0.25	0.66	0.42	2.32

Table 7: *Estimated lifetime cancer risk (ELCR) for individuals attributable to the intake of ambient $PM_{2.5}$.*

		<1	1 to <2	2 to <3	3 to <6	6 to <11	11 to <16	16 to <21	21 to <61	61 to <71	71 >
December	Average	2,64E-03	1,72E-03	1,17E-03	6,45E-04	2,21E-04	6,92E-05	4,35E-05	3,49E-05	3,49E-05	3,49E-05
	Max	4,51E-03	2,94E-03	2,01E-03	1,10E-03	3,78E-04	1,18E-04	7,45E-05	5,97E-05	5,97E-05	5,97E-05
	Min	1,17E-03	7,62E-04	5,20E-04	2,86E-04	9,80E-05	3,07E-05	1,93E-05	1,55E-05	1,55E-05	1,55E-05
January	Average	1,00E-03	6,53E-04	4,46E-04	2,45E-04	8,40E-05	2,63E-05	1,66E-05	1,33E-05	1,33E-05	1,33E-05
	Max	1,90E-03	1,24E-03	8,43E-04	4,64E-04	1,59E-04	4,98E-05	3,13E-05	2,51E-05	2,51E-05	2,51E-05
	Min	4,55E-04	2,97E-04	2,02E-04	1,11E-04	3,81E-05	1,19E-05	7,52E-06	6,02E-06	6,02E-06	6,02E-06
February	Average	1,28E-03	8,33E-04	5,68E-04	3,13E-04	1,07E-04	3,35E-05	2,11E-05	1,69E-05	1,69E-05	1,69E-05
	Max	3,62E-03	2,36E-03	1,61E-03	8,86E-04	3,03E-04	9,50E-05	5,98E-05	4,79E-05	4,79E-05	4,79E-05
	Min	2,13E-04	1,39E-04	9,46E-05	5,21E-05	1,78E-05	5,59E-06	3,52E-06	2,82E-06	2,82E-06	2,82E-06
March	Average	6,72E-04	4,38E-04	2,99E-04	1,64E-04	5,63E-05	1,76E-05	1,11E-05	8,89E-06	8,89E-06	8,89E-06
	Max	1,75E-03	1,14E-03	7,77E-04	4,28E-04	1,46E-04	4,59E-05	2,89E-05	2,31E-05	2,31E-05	2,31E-05
	Min	2,26E-04	1,47E-04	1,01E-04	5,54E-05	1,89E-05	5,94E-06	3,74E-06	2,99E-06	2,99E-06	2,99E-06
April	Average	2,11E-04	1,38E-04	9,40E-05	5,17E-05	1,77E-05	5,55E-06	3,49E-06	2,80E-06	2,80E-06	2,80E-06
	Max	4,00E-04	2,60E-04	1,78E-04	9,78E-05	3,35E-05	1,05E-05	6,60E-06	5,29E-06	5,29E-06	5,29E-06
	Min	1,14E-04	7,43E-05	5,07E-05	2,79E-05	9,54E-06	2,99E-06	1,88E-06	1,51E-06	1,51E-06	1,51E-06
May	Average	5,95E-04	3,88E-04	2,65E-04	1,46E-04	4,98E-05	1,56E-05	9,83E-06	7,87E-06	7,87E-06	7,87E-06
	Max	1,15E-03	7,49E-04	5,11E-04	2,81E-04	9,62E-05	3,02E-05	1,90E-05	1,52E-05	1,52E-05	1,52E-05
	Min	5,49E-05	3,58E-05	2,44E-05	1,34E-05	4,60E-06	1,44E-06	9,07E-07	7,27E-07	7,27E-07	7,27E-07
June	Average	3,62E-04	2,36E-04	1,61E-04	8,85E-05	3,03E-05	9,49E-06	5,97E-06	4,78E-06	4,78E-06	4,78E-06
	Max	8,60E-04	5,60E-04	3,82E-04	2,10E-04	7,20E-05	2,26E-05	1,42E-05	1,14E-05	1,14E-05	1,14E-05
	Min	8,39E-05	5,46E-05	3,73E-05	2,05E-05	7,02E-06	2,20E-06	1,38E-06	1,11E-06	1,11E-06	1,11E-06
$PM_{2.5}$	Average	8,37E-04	5,45E-04	3,72E-04	2,05E-04	7,00E-05	2,20E-05	1,38E-05	1,11E-05	1,11E-05	1,11E-05
	Max	4,51E-03	2,94E-03	2,01E-03	1,10E-03	3,78E-04	1,18E-04	7,45E-05	5,97E-05	5,97E-05	5,97E-05
	Min	5,49E-05	3,58E-05	2,44E-05	1,34E-05	4,60E-06	1,44E-06	9,07E-07	7,27E-07	7,27E-07	7,27E-07

of days and "Moderate" for only 0.26%, indicating infrequent short-term peaks—likely linked to transient meteorological conditions—that did not pose significant health risks to the general population.

Except for PM, which had an AQI ranging from moderate to very unhealthy, the overall air quality throughout the research was typically at a moderate level (Table 5). Although the AQI offers a simplified understanding of the health risks associated with exposure to a specific air pollutant, it does not serve as an air quality guideline. While concentration time series display unprocessed pollutant levels, the AQI integrates this data into a standardized scale that corresponds to health-effect categories. Each pollutant's concentration is converted into a sub-index, and the highest daily value is used to determine the pollutant driving health risk—a detail not apparent from concentration data alone. For instance, even if $PM_{2.5}$ remains at moderate levels, a short-term increase in O_3 may determine the AQI, signalling the need for ozone-focused management strategies. As such, the AQI graph provides an immediate and intuitive summary of air quality trends, exceedances, and pollutant priorities for communication with decision-makers and the public.

Health risk assessment

This research assessed health risks associated with $PM_{2.5}$ and PM_{10} exposure by estimating the extra lifetime cancer risk and non-carcinogenic risk. We used Equation (3) to find the excess lifetime cancer risk (ELCR), Equation (3) to find the lifetime average daily dose (LADD) (µg/kg.day), and Equation (6) to find the HQ (Supplementary material, Table S2, listing risk assessment parameters for different age groups including inhalation rates, exposure times, and RfDs).

ELCR values for $PM_{2.5}$ exposure ranged from 1.11×10^{-5} to 8.37×10^{-4}, exceeding the USEPA acceptable risk threshold (1.0×10^{-6}) across all age groups, with the highest values observed during the winter months. HQ values remained below 1 for both $PM_{2.5}$ and PM_{10} except in December, indicating tolerable non-carcinogenic risk for most of the year (Table 6). In this investigation, the estimated ELCR values resulting from $PM_{2.5}$ exposure varied from 1.11×10^{-5} to 8.37×10^{-4}, significantly exceeding the upper threshold of the acceptable risk range established by the USEPA. The monthly average concentrations of $PM_{2.5}$ consistently resulted in ELCR values that significantly exceeded the threshold of 1.0×10^{-6}, highlighting a considerable public health issue. In December, the highest average ELCRs were noted, especially among younger age groups, with values that notably surpassed the USEPA threshold of 1.0×10^{-6}, indicating an increased cancer risk associated with prolonged exposure to $PM_{2.5}$. The values exhibit a consistent decline as age groups increase, alongside reduced concentrations during warmer months such as April and June. This highlights a vulnerability related to seasonality and demographics that must be considered in public health policies. In comparison to other studies, our results indicate an elevated cancer risk. These findings suggest a potential carcinogenic risk from prolonged exposure to ambient $PM_{2.5}$ in the study area, particularly for sensitive populations, which is consistent with previous studies reporting elevated health risks associated with fine particulate matter exposure in urban environments (Hamra et al. 2014; Chen and Hoek 2020).

The lifetime average daily dose of $PM_{2.5}$ in Bou-Ismail was between 0.26 and 21.72 µg/kg.day, with 4.03 µg/kg.day being the average. Measurements of PM_{10} indicated that the lifetime average daily dose (µg/kg.day) ranged from 1.32 to 52.77 µg/kg.day, with an average of 9.17 µg/kg.day (Supplement materiel, Table S6). Table 6 illustrates that the mean health quotient (HQ) for $PM_{2.5}$ in Bou-Ismail was 0.59, with a range of 0.15 to 1.86. PM_{10}, it was 0.40, with a range of 0.13 to 1.03. The higher values for $PM_{2.5}$ and PM_{10} were recorded only in December (HQ>1), while the rest of the months show HQ<1. People face minimal or no non-cancer danger when HQ is less than 1, according to Saju (Saju et al. 2023). In December, HQ values surpassed 1, suggesting a potential non-carcinogenic risk during winter; however, they remained below 1 in all other months, indicating acceptable risk levels for the majority of the study period.

The high HQ values observed in December are likely due to increased emissions from home heating, stagnant air, and temperature inversions, which contribute to higher PM levels in the air (Bounakhla et al. 2023; Amare et al. 2024). Urban areas commonly observe seasonal effects, as adverse meteorological conditions intensify wintertime pollution episodes (Bamola et al. 2024). The observed HQ peak in colder months corresponds with findings from other studies, highlighting the significance of seasonal air quality regulation. The consistently higher HQ values of $PM_{2.5}$ compared to PM_{10} are due to its smaller size, which allows it to go deeper into the lungs and cause more health problems. Research indicates that $PM_{2.5}$ is a significant contributor to respiratory problems, cardiovascular issues, and long-term health concerns, primarily due to its composition and reaction mechanisms. While HQ values for the majority of months stayed within acceptable thresholds, the exceedance in December signifies a temporary yet notable exposure risk, especially for vulnerable populations. The findings indicate that prioritising specific mitigation strategies, such as emission reductions during winter, is essential for preventing health impacts in vulnerable communities (Heydari et al. 2019; Khoshakhlagh et al. 2023).

Conclusion

The paper presents the first simultaneous hourly for air quality parameters measurement of O_3, SO_2, NO, NO_2, CO, and $PM_{2.5}$ and PM_{10} concentrations in the Bou-Ismail area, using Airpointer (Recordum, Austria) from December 15 to March 31, 2016 (Winter) and from April 1 to June 29, 2016 (Spring). There were correlations between NO, NO_2, $PM_{2.5}$, PM_{10}, and SO_2, suggesting that these pollutants come from petrol and sulfur-containing vehicle exhaust. Another high correlation between ozone and temperature supports the photochemical synthesis of ozone. The negative relationship between ozone (O_3), NO, and NO_2 suggests that NO and NO_2 contribute to the depletion of O_3.

Winter peaks in $PM_{2.5}$ and PM_{10} drove AQI exceedances on over 42 of 196 days, indicating significant health risks to vulnerable groups. Multivariate analyses (PCA and HCA) revealed four coherent source–meteorology groupings: traffic emissions, temperature-dependent photochemistry, atmospheric stability, and regional transport. Back-trajectory pathways linked critical pollution episodes to air masses originating from the Atlantic, Mediterranean, Saharan, and eastern Algerian regions, explaining the observed temporal and spatial variability. The health risk assessment revealed that the monthly ELCR for $PM_{2.5}$ consistently exceeded 1×10^{-6} and HQ > 1 during the winter months, underscoring elevated carcinogenic and non-carcinogenic risks. These integrated findings underscore the need for seasonally targeted emission controls—particularly on traffic—and the importance of enhanced public health advisories, such as mask use during high-pollution days. Future work should incorporate non-linear photochemical modelling and expanded PM_{10} toxicity data to refine risk assessments and policy interventions.

Compliance with ethical standards

Conflicts of interest

The authors declare no conflict of interest.

Data availability statements

The datasets generated during and/or analysed during the current study are available from the corresponding author upon reasonable request.

Funding

Not applicable.

Credit author statement

Adlane Tahar: Conceptualization, writing.
Abdelkader Lemou: Conceptualization, writing.
Lyes Rabhi: Writing, reviewing.
Nabila Cherifi: Reviewing.
Riad Ladji: Reviewing.

References

Ait Bouh H, Bounakhla M, Benyaich F, Noack Y, Tahri M, Foudeil S (2023) Seasonal Variation of Mass Concentration and Chemical Composition of $PM_{2.5}$ and PM_{10}, Source Identification and Human Health Risk Assessment in Meknes City in Morocco. Aerosol Science and Engineering 7(2):151–168. https://doi.org/10.1007/s41810-022-00169-y

Amare AN, Sorsa S, Gebremariam Z (2024) Levels and health risk assessments of particulate matter and inorganic gaseous pollutants in urban and industrial areas of Hawassa city, Ethiopia. Heliyon 10(13):e33286. https://doi.org/10.1016/j.heliyon.2024.e33286

Bamola S, Goswami G, Dewan S, Goyal I, Agarwal M, Dhir A, Lakhani A (2024) Characterising temporal variability of $PM_{2.5}$/PM_{10} ratio and its correlation with meteorological variables at a sub-urban site in the Taj City. Urban Climate 53:101763. https://doi.org/10.1016/j.uclim.2023.101763

Benchrif A, Tahri M, Khalfaoui O, Baghdad B, Bounakhla M, Cachier H (2025) Aerosols in Northern Morocco (Part 4): Seasonal Chemical Signatures of $PM_{2.5}$ and PM_{10}. Atmosphere 16(8). https://doi.org/10.3390/atmos16080982

Bounakhla Y, Benchrif A, Costabile F, Tahri M, El Gourch B, El Hassan EK, Zahry F, Bounakhla M (2023) Overview of PM_{10}, $PM_{2.5}$ and BC and Their Dependent Relationships with Meteorological Variables in an Urban Area in Northwestern Morocco. Atmosphere 14(1). https://doi.org/10.3390/atmos14010162

Cai C, Avise J, Kaduwela A, DaMassa J, Warneke C, Gilman JB, Kuster W, de Gouw J, Volkamer R, Stevens P, Lefer B, Holloway JS, Pollack IB, Ryerson T, Atlas E, Blake D, Rappenglueck B, Brown SS, Dube WP (2019) Simulating the Weekly Cycle of NO_x-VOC-HOx-O_3 Photochemical System in the South Coast of California During CalNex-2010 Campaign. Journal of Geophysical Research: Atmospheres 124(6):3532–3555. https://doi.org/10.1029/2018JD029859

Chen H, Li Q, Kaufman JS, Wang J, Copes R, Su Y, Benmarhnia T (2018) Effect of air quality alerts on human health: a regression discontinuity analysis in Toronto, Canada. The Lancet Planetary Health 2(1):e19–e26. https://doi.org/10.1016/S2542-5196(17)30185-7

Chen J, Hoek G (2020) Long-term exposure to PM and all-cause and cause-specific mortality: A systematic review and meta-analysis. Environment International 143:105974. https://doi.org/10.1016/j.envint.2020.105974

Contini D, Cesari D, Donateo A, Chirizzi D, Belosi F (2014) Characterization of PM_{10} and $PM_{2.5}$ and Their Metals Content in Different Typologies of Sites in South-Eastern Italy. Atmosphere 5(2):435–453. https://doi.org/10.3390/atmos5020435

Cusack M, Pérez N, Pey J, Alastuey A, Querol X (2013) Source apportionment of fine PM and sub-micron particle number concentrations at a regional background site in the western Mediterranean: a 2.5 year study. Atmospheric Chemistry and Physics 13(10):5173–5187. https://doi.org/10.5194/acp-13-5173-2013

Cusick M, Rowland ST, DeFelice N (2023) Impact of air pollution on running performance. Sci Rep 13(1):1832. https://doi.org/10.1038/s41598-023-28802-x

De Ferreyro Monticelli D, Santos JM, Goulart EV, Mill JG, Kumar P, Reis Jr. NC (2021) A review on the role of dispersion and receptor models in asthma research. Environmental Pollution 287:117529. https://doi.org/10.1016/j.envpol.2021.117529

Di Vaio P, Magli E, Barbato F, Caliendo G, Cocozziello B, Corvino A, De Marco A, Fiorino F, Frecentese F, Onorati G, Saccone I,

Santagada V, Soggiu ME, Severino B, Perissutti E (2016) Chemical Composition of PM_{10} at Urban Sites in Naples (Italy). Atmosphere 7(12). https://doi.org/10.3390/atmos7120163

Gladson LA, Cromar KR, Ghazipura M, Knowland KE, Keller CA, Duncan B (2022) Communicating respiratory health risk among children using a global air quality index. Environment International 159:107023. https://doi.org/10.1016/j.envint.2021.107023

Greene NA, Morris VR (2006) Assessment of Public Health Risks Associated with Atmospheric Exposure to $PM_{2.5}$ in Washington, DC, USA. IJERPH 3(1):86–97. https://doi.org/10.3390/ijerph2006030010

Grivas G, Chaloulakou A (2006) Artificial neural network models for prediction of PM_{10} hourly concentrations, in the Greater Area of Athens, Greece. Atmospheric Environment 40(7):1216–1229. https://doi.org/10.1016/j.atmosenv.2005.10.036

Guarnieri M, Balmes JR (2014) Outdoor air pollution and asthma. The Lancet 383(9928):1581–1592. https://doi.org/10.1016/S0140-6736(14)60617-6

Hamra G, Guha N, Cohen A, Laden F, Samet J, Vineis P, Forastiere F, Saldiva P, Yorifuji T, Loomis D (2014) Outdoor Particulate Matter Exposure and Lung Cancer: A Systematic Review and Meta-Analysis. Environmental health perspectives 122. https://doi.org/10.1289/ehp.1408092

Han H, Liu J, Shu L, Wang T, Yuan H (2020) Local and synoptic meteorological influences on daily variability in summertime surface ozone in eastern China. Atmospheric Chemistry and Physics 20(1):203–222. https://doi.org/10.5194/acp-20-203-2020

Heydari G, Taghizdeh F, Fazlzadeh M, Jafari AJ, Asadgol Z, Mehrizi EA, Moradi M, Arfaeinia H (2019) Levels and health risk assessments of particulate matters ($PM_{2.5}$ and PM_{10}) in indoor/outdoor air of waterpipe cafés in Tehran, Iran. Environmental Science and Pollution Research 26(7):7205–7215. https://doi.org/10.1007/s11356-019-04202-5

Iglesias-Suarez F, Badia A, Fernandez RP, Cuevas CA, Kinnison DE, Tilmes S, Lamarque J-F, Long MC, Hossaini R, Saiz-Lopez A (2020) Natural halogens buffer tropospheric ozone in a changing climate. Nat Clim Chang 10(2):147–154. https://doi.org/10.1038/s41558-019-0675-6

Khoshakhlagh AH, Mohammadzadeh M, Morais S (2023) Air quality in Tehran, Iran: Spatio-temporal characteristics, human health effects, economic costs and recommendations for good practice. Atmospheric Environment: X 19:100222. https://doi.org/10.1016/j.aeaoa.2023.100222

Lanzafame R, Monforte P, Patanè G, Strano S (2015) Trend Analysis of Air Quality Index in Catania from 2010 to 2014. Energy Procedia 82:708–715. https://doi.org/10.1016/j.egypro.2015.11.796

Lemou A, Rabhi L, Cherifi N, Ladji R, Yassaa N (2020) Temporal variation of PM_{10}, $PM_{2.5}$ and gaseous pollutants (NO_x, SO_2) particles suspended in the atmosphere of an urban sit in Bou-Ismail. Algerian Journal of Environmental Science and Technology 6(3):1537–1541

Li Y, Yin S, Yu S, Bai L, Wang X, Lu X, Ma S (2021) Characteristics of ozone pollution and the sensitivity to precursors during early summer in central plain, China. Journal of Environmental Sciences 99:354–368. https://doi.org/10.1016/j.jes.2020.06.021

Ma T, Duan F, He K, Qin Y, Tong D, Geng G, Liu X, Li H, Yang S, Ye S, Xu B, Zhang Q, Ma Y (2019a) Air pollution characteristics and their relationship with emissions and meteorology in the Yangtze River Delta region during 2014–2016. Journal of Environmental Sciences 83:8–20. https://doi.org/10.1016/j.jes.2019.02.031

Ma T, Duan F, He K, Qin Y, Tong D, Geng G, Liu X, Li H, Yang S, Ye S, Xu B, Zhang Q, Ma Y (2019b) Air pollution characteristics and their relationship with emissions and meteorology in the Yangtze River Delta region during 2014–2016. Journal of Environmental Sciences 83:8–20. https://doi.org/10.1016/j.jes.2019.02.031

Mehdi Qasemi MF Mojtaba Afsharnia, Ahmad Zarei, Allahdadi M (2019) Non-carcinogenic risk assessment to human health due to intake of fluoride in the groundwater in rural areas of Gonabad and Bajestan, Iran: A case study. Human and Ecological Risk Assessment: An International Journal 25(5):1222–1233. https://doi.org/10.1080/10807039.2018.1461553

Munir S, Habeebullah TM, Seroji AR, Gabr SS, Mohammed AMF, Morsy EA (2013) Quantifying temporal trends of atmospheric pollutants in Makkah (1997–2012). Atmospheric Environment 77:647–655. https://doi.org/10.1016/j.atmosenv.2013.05.075

Mushtaq Z, Bangotra P, Gautam AS, Sharma M, Suman, Gautam S, Singh K, Kumar Y, Jain P (2024) Satellite or ground-based measurements for air pollutants ($PM_{2.5}$, PM_{10}, SO_2, NO_2, O_3) data and their health hazards: which is most accurate and why? Environ Monit Assess 196(4):342. https://doi.org/10.1007/s10661-024-12462-z

OJRA (2006) Décret exécutif n° 06-02 du 7 Dhou El Hidja 1426 correspondant au 7 janvier 2006 définissant les valeurs limites, les seuils d'alerte et les objectifs de qualité de l'air en cas de pollution atmosphérique.

Pusede SE, Steiner AL, Cohen RC (2015) Temperature and Recent Trends in the Chemistry of Continental Surface Ozone. Chem Rev 115(10):3898–3918. https://doi.org/10.1021/cr5006815

Querol X, Alastuey A, Pey J, Cusack M, Pérez N, Mihalopoulos N, Theodosi C, Gerasopoulos E, Kubilay N, Koçak M (2009) Variability in regional background aerosols within the Mediterranean. Atmospheric Chemistry and Physics 9(14):4575–4591. https://doi.org/10.5194/acp-9-4575-2009

Querol X, Alastuey A, Ruiz CR, Artiñano B, Hansson HC, Harrison RM, Buringh E, Brink HM [ten, Lutz M, Bruckmann P, Straehl P, Schneider J (2004) Speciation and origin of PM_{10} and $PM_{2.5}$ in selected European cities. Atmospheric Environment 38(38):6547–6555. https://doi.org/10.1016/j.atmosenv.2004.08.037

Rabhi L, Lemou A, Ladji R, Khedidji S, Bonnaire N, Sciare J, Yassaa N (2024) Size distribution of water-soluble ions and carbon content in the Southwest Mediterranean Basin: results from the ChArMEx project. Air Qual Atmos Health. https://doi.org/10.1007/s11869-024-01614-2

Rani Hemamalini R, Vinodhini R, Shanthini B, Partheeban P, Charumathy M, Cornelius K (2022) Air quality monitoring and forecasting using smart drones and recurrent neural network for sustainable development in Chennai city. Sustainable Cities and Society 85:104077. https://doi.org/10.1016/j.scs.2022.104077

Rolph G, Stein A, Stunder B (2017) Real-time Environmental Applications and Display sYstem: READY. Environmental Modelling & Software 95:210–228. https://doi.org/10.1016/j.envsoft.2017.06.025

Saju JA, Bari QH, Mohiuddin KABM, Strezov V (2023) Measurement of ambient particulate matter (PM1.0, $PM_{2.5}$ and PM_{10}) in Khulna City of Bangladesh and their implications for human health. Environmental Systems Research 12(1):42. https://doi.org/10.1186/s40068-023-00327-2

Santus P, Russo A, Madonini E, Allegra L, Blasi F, Centanni S, Miadonna A, Schiraldi G, Amaducci S (2012) How air pollution influences clinical management of respiratory diseases. A case-crossover study in Milan. Respir Res 13(1):95. https://doi.org/10.1186/1465-9921-13-95

Sarkar N, Gupta R, Keserwani PK, Govil MC (2022) Air Quality Index prediction using an effective hybrid deep learning model. Environmental Pollution 315:120404. https://doi.org/10.1016/j.envpol.2022.120404

Seo J, Park D-SR, Kim JY, Youn D, Lim YB, Kim Y (2018) Effects of meteorology and emissions on urban air quality: a quantitative statistical approach to long-term records (1999–2016) in Seoul, South Korea. Atmospheric Chemistry and Physics 18(21):16121–16137. https://doi.org/10.5194/acp-18-16121-2018

Shen Y, Meng H, Yao X, Peng Z, Sun Y, Zhang J, Gao Y, Feng L, Liu X, Gao H (2022) Does Ambient Secondary Conversion or the Prolonged Fast Conversion in Combustion Plumes Cause Severe $PM_{2.5}$ Air Pollution in China? Atmosphere 13(5):673. https://doi.org/10.3390/atmos13050673

Shrestha DL, Solomatine DP (2006) Machine learning approaches for estimation of prediction interval for the model output. Neural Networks 19(2):225–235. https://doi.org/10.1016/j.neunet.2006.01.012

Sidibe A, Sakamoto Y, Murano K, Sato K, Yuba A, Futami M, Koita OA, Traore I, Kajii Y (2022) Chemical Characterization and Health Risk Assessment of Particulate Matter from Household Activities in Bamako, Mali, Western Sub-Saharan Africa. Atmosphere 13(8). https://doi.org/10.3390/atmos13081290

Singh K, Tripathi D (2021) Particulate Matter and Human Health. In: Otsuki T (ed) Environmental Health. IntechOpen

Spandana B, Rao SS, Upadhya AR, Kulkarni P, Sreekanth V (2021) $PM_{2.5}/PM_{10}$ ratio characteristics over urban sites of India. Advances in Space Research 67(10):3134–3146. https://doi.org/10.1016/j.asr.2021.02.008

Tayanç M, Sezen İ, Ünal A, Flores RM, Karanfil S (2022) A holistic approach to the air quality of Konya City, Turkey. Air Quality, Atmosphere & Health 15(6):951–965. https://doi.org/10.1007/s11869-022-01200-4

Thurston GD (2008) Outdoor Air Pollution: Sources, Atmospheric Transport, and Human Health Effects

U.S. EPA (U.S. Environmental Protection Agency) (2009a) Risk assessment guidance for superfund volume 1: Human health evaluation manual (part f, supplemental guidance for dermal risk assessment). Office of Superfund Remediation and Technology Innovation, Washington DC.

U.S. EPA (U.S. Environmental Protection Agency) (2009b) Risk assessment guidance for Superfund vol I: Human health evaluation manual (part F, supplemental guidance for inhalation risk assessment). Office of Superfund Remediation and Technology Innovation, Washington DC.

USEPA (2023) User's Guide for the AMSEPA Regulatory Model (AERMOD), US Environmental Protection Agency

USEPA (2009) Guidelines for the Reporting of Daily Air Quality – the Air Quality Index (AQI). EPA-456/F-09-002

USEPA (2011) Risk Assessment Guidance for Superfund Volume I: Human Health Evaluation Manual (Part F, Supplemental Guidance for Inhalation Risk Assessment)

Valavanidis A, Fiotakis K, Vlahogianni T, Bakeas EB, Triantafillaki S, Paraskevopoulou V, Dassenakis M (2006) Characterization of atmospheric particulates, particle-bound transition metals and polycyclic aromatic hydrocarbons of urban air in the centre of Athens (Greece). Chemosphere 65(5):760–768. https://doi.org/10.1016/j.chemosphere.2006.03.052

Verma MK, Patel A, Sahariah BP, Choudhari JK (2016) Computation of Air Quality Index for Major Cities of Chhattisgarh State. Environmental Claims Journal 28(3):195–205. https://doi.org/10.1080/10406026.2016.1129269

WHO (2022) World health statistics 2022: monitoring health for the SDGs, sustainable development goals. Geneva: World Health Organization

WHO (2005) WHO Air quality guidelines for particulate matter, ozone, nitrogen dioxide and sulfur dioxide. World Health Organization

WHO (2021) WHO global air quality guidelines: particulate matter ($PM_{2.5}$ and PM_{10}), ozone, nitrogen dioxide, sulfur dioxide and carbon monoxide. Geneva: World Health Organization; 2021. Licence: CC BY-NC-SA 3.0 IGO.

Wikuats CFH, Nogueira T, Squizzato R, De Freitas ED, Andrade MDF (2023) Health Risk Assessment of Exposure to Air Pollutants Exceeding the New WHO Air Quality Guidelines (AQGs) in São Paulo, Brazil. IJERPH 20(9):5707. https://doi.org/10.3390/ijerph20095707

Wu C, He H, Song R, Zhu X, Peng Z, Fu Q, Pan J (2023) A hybrid deep learning model for regional O_3 and NO_2 concentrations prediction based on spatiotemporal dependencies in air quality monitoring network. Environmental Pollution 320:121075. https://doi.org/10.1016/j.envpol.2023.121075

Xiao C, Chang M, Guo P, Gu M, Li Y (2020) Analysis of air quality characteristics of Beijing–Tianjin–Hebei and its surrounding air pollution transport channel cities in China. Journal of Environmental Sciences 87:213–227. https://doi.org/10.1016/j.jes.2019.05.024

Yunesian M, Rostami R, Zarei A, Fazlzadeh M, Janjani H (2019) Exposure to high levels of $PM_{2.5}$ and PM_{10} in the metropolis of Tehran and the associated health risks during 2016–2017. Microchemical Journal 150:104174. https://doi.org/10.1016/j.microc.2019.104174

Zhang G, Sun Y, Xu W, Wu L, Duan Y, Liang L, Li Y (2023) Identifying the O_3 chemical regime inferred from the weekly pattern of atmospheric O_3, CO, NO_x, and PM_{10}: Five-year observations at a center urban site in Shanghai, China. Science of The Total Environment 888:164079. https://doi.org/10.1016/j.scitotenv.2023.164079

Zhang J, Li S (2022) Air quality index forecast in Beijing based on CNN-LSTM multi-model. Chemosphere 308:136180. https://doi.org/10.1016/j.chemosphere.2022.136180

Zhang X, Shi M, Li Y, Pang R, Xiang N (2018) Correlating $PM_{2.5}$ concentrations with air pollutant emissions: A longitudinal study of the Beijing-Tianjin-Hebei region. Journal of Cleaner Production 179:103–113. https://doi.org/10.1016/j.jclepro.2018.01.072

Zhou X, Cao Z, Ma Y, Wang L, Wu R, Wang W (2016) Concentrations, correlations and chemical species of $PM_{2.5}$/PM_{10} based on published data in China: Potential implications for the revised particulate standard. Chemosphere 144:518–526. https://doi.org/10.1016/j.chemosphere.2015.09.003

Supplementary material

Supplementary material can be accessed at https://cleanairjournal.org.za/article/view/21575